



Operando X-ray absorption and infrared fuel cell spectroscopy

Emily A. Lewis^a, Ian Kendrick^a, Qingying Jia^b, Corey Grice^c, Carlo U. Segre^b, Eugene S. Smotkin^{a,*}

^a Department of Chemistry and Chemical Biology, Northeastern University, Boston, MA 02115, United States

^b Physics Division, Department of Biological, Chemical and Physical Sciences, Illinois Institute of Technology, Chicago, IL 60616, United States

^c NuVant Systems Inc., Crown Point, IN 46307, United States

ARTICLE INFO

Article history:

Received 20 July 2011

Received in revised form 23 July 2011

Accepted 23 July 2011

Available online 29 July 2011

Keywords:

Fuel cell

Membrane electrode assembly

Operando spectroscopy

X-ray absorption spectroscopy

Infrared spectroscopy

Stark tuning

Platinum

Nickel

XANES

ABSTRACT

A polymer electrolyte fuel cell enables operando X-ray absorption and infrared spectroscopy of the membrane electrode assembly catalytic layer with flowing fuel and air streams at controlled temperature. Time-dependent X-ray absorption near edge structure spectra of the Pt and Ni edge of Pt based catalysts of an air-breathing cathode show that catalyst restructuring, after a potential step, has time constants from minutes to hours. The infrared Stark tuning plots of CO adsorbed on Pt at 100, 200, 300 and 400 mV vs. hydrogen reference electrode were obtained. The Stark tuning plots of CO adsorbed at 400 mV exhibit a precipitous drop in frequency coincident with the adsorption potential. The turn-down potential decreases relative to the adsorption potential and is approximately constant after 300 mV. These Stark tuning characteristics are dependent to potential dependent adsorption site selection by CO and competitive adsorption processes.

© 2011 Elsevier Ltd. All rights reserved.

1. Introduction

Because the active state of a catalyst exists only during catalysis [1], the characterization of catalysts should be done under standard device operating conditions: catalysts, incorporated into membrane electrode assemblies (MEAs), are exposed to flowing reactant streams within flow fields operating from 60 to 80 °C. This work focuses on platinum-based catalysts of polymer electrolyte reactors. Such reactors have applications in organic synthesis [2–9], environmental remediation [10,11] and energy conversion [12]. The MEA, a polymer electrolyte membrane sandwiched between catalytic layers contacting porous carbon paper or cloth gas diffusion layers, is optimized for reactant transport and electronic conduction. MEA fabrication methods have been reviewed [13]. Briefly, inks are prepared by dispersing catalysts in solubilized ionomer. The inks are either deposited onto the carbon gas diffusion layers followed by hot pressing to the membrane (i.e., 5-layer MEA), or directly deposited onto a heated membrane surface (i.e., 3-layer MEA). The catalyst layers (carbon supported or metal blacks [14]) are a blend of ionomer, catalyst particles and, in some cases, teflon dispersion. In an operating MEA, the catalyst particles are wetted with a sub- μm layer of ionomer that conducts protons and

enhances catalysis [15]. Operando characterization of MEA catalytic layers requires an absence of supplemental electrolytes: aqueous electrolytes (e.g., H_2SO_4 or HClO_4) contribute mobile anion adsorbates, and preclude fuel cell operation at the high end of relevant temperatures (e.g., 70–90 °C).

Proper cell design is the key challenge to operando spectroscopy. In addition to a “real world” catalyst environment, standard electrochemical cell design principles must be adhered to, including equal resistance between any points of the working electrode surface to an auxiliary electrode surface, and a high impedance reference electrode [16]. Stainless steel should be avoided. It includes iron, nickel and chromium, which fluoresce at energies similar to the edge energies of Pt based catalysts.

Viswanathan et al. [17] and Stoupin et al. [18] introduced operando X-ray absorption spectroscopy (XAS) of hydrogen and liquid feed direct methanol fuel cells respectively using the cell in Fig. 1. This cell design was used by Principi et al. [19] in low Pt loading XAS studies. Palladium at the cathode mitigates interference when studying Pt based catalyst edge energies. A recently reported operando X-ray absorption cell describes a design that mitigates this problem [20].

The resistance between the anode and cathode catalytic layers of a membrane electrode assembly is governed by a uniform polymer electrolyte membrane thickness (ca. 7 mil for Nafion 117) [21]. The counter electrode to the working electrode of interest serves as both the auxiliary and the reference electrode

* Corresponding author. Tel.: +1 617 373 7526.

E-mail address: e.smotkin@neu.edu (E.S. Smotkin).

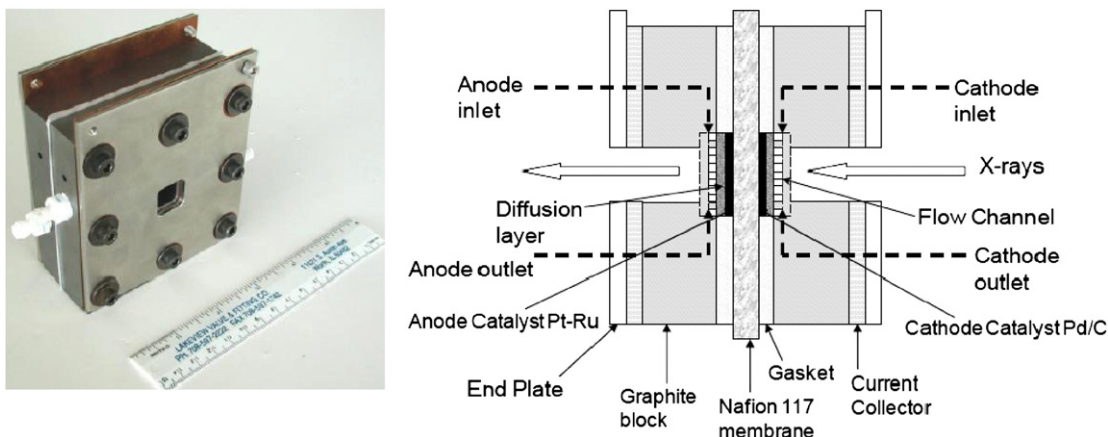


Fig. 1. Operando spectroscopy fuel cell and schematic (from Ref. [17]).

(counter-reference electrode) [22]. Counter-reference electrodes are also used in two-electrode microelectrode studies where polarization of a standard reference electrode is unlikely with sub- μ A working electrode currents [23]. A hydrogen counter-reference is often used for acquisition of direct methanol fuel cell anode polarization curves [24]. Pure water can be delivered to the counter-reference electrode when obtaining anode polarization curves because hydrogen evolved at the counter electrode poises [25] as the counter electrode to the hydrogen electrode potential: The hydrogen ion activity is set by the Nafion equivalent weight (e.g., 1100 g for Nafion 117) and state of hydration. The high acidity of Nafion is attributed to the CF_2 group alpha to the sulfonic acid exchange group [26]. Although use of the counter-reference has drawbacks at high currents, the alternative of developing a 3rd elec-

trode as a reference electrode is far more complex than correcting for reference electrode polarization losses using current interrupt or impedance measurements. On a practical level, the use of the fuel cell counter-reference affords greater reproducibility between laboratories. This work focuses on steady state conditions at fixed potentials where polarization of the counter-reference electrode is negligible.

A number of operando XAS [27–34] studies followed that of Viswanathan with many focused on the oxidation state of the metal components. All found that at relevant fuel cell anode operating potentials, platinum is metallic. The oxidation of CO was studied both on Pt [31], and PtRu [27,30,35,36], confirming the electronic benefits of Ru as a co-catalyst for CO oxidation. Studies of adsorbed oxygen reduction reaction intermediates on fuel

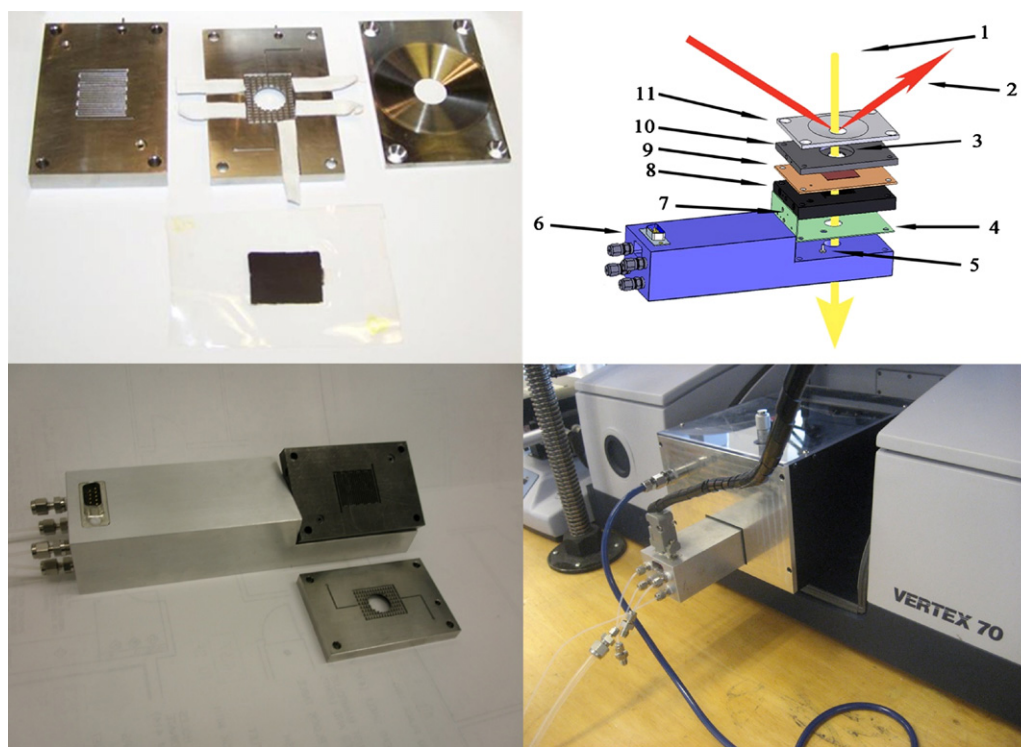


Fig. 2. IR-XAS cell. Top left panel: bottom and top flow field with wicking material (white strips). The top plate shows the bevel required for fluorescence studies. The MEA is shown in lower part of panel. Top right: (1) transmission X-ray path, (2) reflectance IR or fluorescence X-ray path, (3) CaF_2 window housing, (4) Teflon gasket, (5) gas outlet insert, (6) slider housing, (7) thermocouple/heater cartridge port, (8) lower flow field, (9) MEA, (10) upper flow field, and (11) top plate. Bottom left: partially assembled IR-XAS cell with DE9 connector for electrodes, heater cartridge and resistance temperature detector. Bottom right panel: cell installed in Pike diffuse reflectance accessory in a Bruker (Billerica, MA) Vertex 70 FTIR Spectrometer.

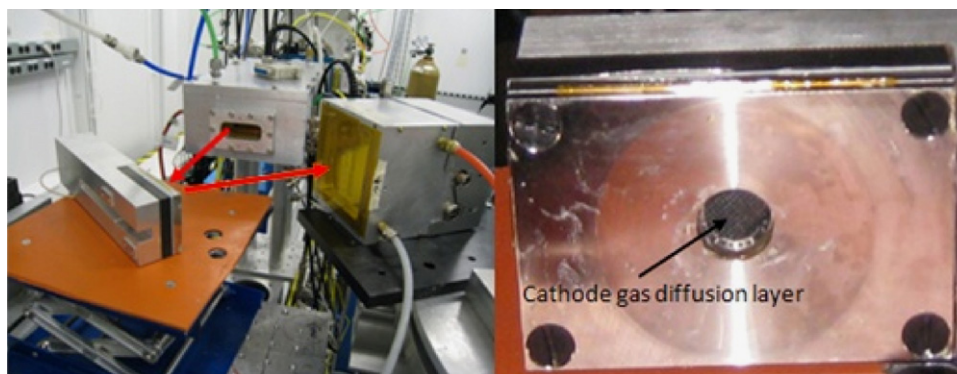


Fig. 3. IR-XAS cell at MRCAT beam line, Argonne National Laboratory.

cell catalysts show that adsorption is both potential-dependent and site-specific [27,37–40].

2. Experimental

2.1. Cell design

The Viswanathan cell was limited to transmission X-ray absorption measurements. The new cell (Fig. 2) combines features of the Viswanathan cell [17] with the operando specular reflectance infrared (IR) cell reported by Fan et al. [41]. This IR-XAS cell enables operando XAS (in transmission and fluorescence) and specular reflectance FTIR spectroscopy without the need for extraction of the MEA and interchange of cells. The top flow field (Fig. 2, top right), accommodates a CaF_2 window for IR reflectance studies [41–43]. The CaF_2 window can be removed when the working electrode of interest is an air-breathing electrode. An advantage of fluorescence X-ray absorption is that the beam intensity is not attenuated by the lower graphite flow field (component 8). The IR-XAS cell is designed for use with commercially available IR diffuse reflection accessories (Fig. 2, bottom right). Fig. 2 (bottom left) shows the lower flow field, the top flow field (with wicking material for condensed water removal) and the top plate.

The fuel cell housing bolts to a slider assembly (Fig. 2, component 6) that provides a 9-pin connector for cell electronics and temperature control. Swagelok fittings are used for fuel and oxidant delivery and exhaust. A wide beveled (not viewable) slot beneath the cell (Fig. 2, bottom left) enables variable angle X-ray transmission spectroscopy. Fig. 3 shows the cell as an air breathing fuel cell at the MRCAT beam line at the Argonne National Laboratory. The source beam (arrow) passes through the cathode gas diffusion layer on the front face of the cell (Fig. 3, right photo). Fluorescence is detected by the Lytle detector.

The slot on the underside also ensures precise positioning of the cell under the integrated mirrors of the Diffuse-IR accessory (Pike Technologies, Madison, WI) (Fig. 2, bottom right). A 158° bevel angle on the top plate maximizes the collection of the scattered signal. A pin-style upper flow field optimizes flow distribution around the CaF_2 window inset. Fig. 4 shows a polarization curve (.04 mV/min) of the IR-XAS cell. Humidified H_2 (50 sccm) and air (250 sccm) were delivered to the counter and working electrodes respectively at 50°C .

2.2. MEA preparation

Catalyst inks, prepared by the method of Wilson [44], were directly applied to Nafion (4 mg/cm^2 of metal blacks at the working electrode and the same loading of Pt or Pd at the counter-reference electrode) immobilized on a heated vacuum table (NuVant Systems,

Crown Point, IN) maintained at 70°C . These loadings are typical for unsupported catalysts often used in liquid feed direct oxidation fuel cells [24]. Carbon paper (Toray Industries, Tokyo, Japan) blocked with Vulcan XC-72 carbon was used as a current collector at both electrodes. The MEA was conditioned [17] by cycling from 800 to 600 mV (40 mV/min) for five cycles with humidified H_2 (50 sccm) at the counter-reference electrode and air (250 sccm) at the windowed working electrode. The air was purged from the working electrode with N_2 , followed by further conditioning by cyclic voltammetry (CV) over the range 0–1.2 V (100 mV/s) for fifty scans.

2.3. X-ray absorption spectroscopy

The cathode gas diffusion layer was exposed to ambient air (i.e., CaF_2 window not installed) while humidified hydrogen was delivered to the Pd counter-reference electrode. After an initial 1-h conditioning period [45], the fuel cell was disconnected, brought to the experimental station, reconnected to the humidified gas feeds, and held at a potential of 530 mV. Time-dependent XANES were sequentially acquired at 2 min intervals and then subtractively normalized to the reference spectrum, which was obtained at 0 V after completion of the time sequence.

2.4. Operando infrared spectroscopy

Spectra from 800 to 4000 cm^{-1} , at 4 cm^{-1} resolution, were acquired with a Vertex 70 Spectrometer (Bruker instruments, Bil-

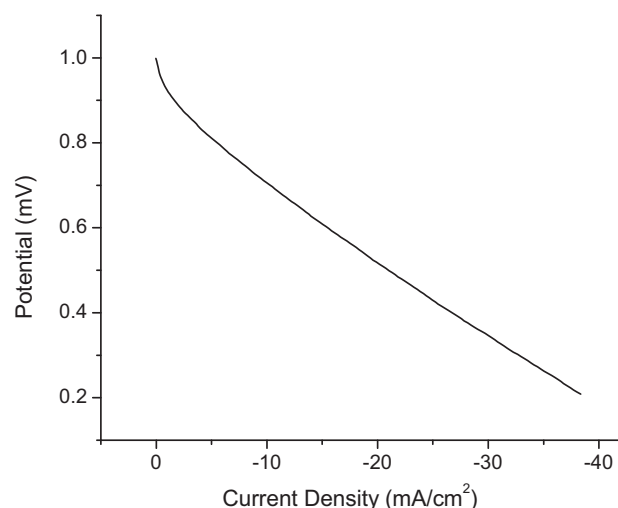


Fig. 4. IR-XAS fuel cell polarization curve.

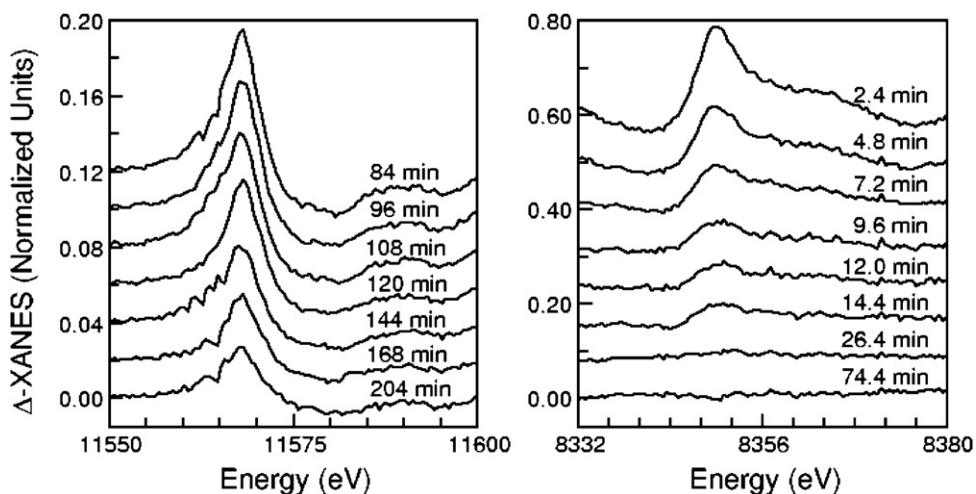


Fig. 5. Time-dependent XANES at 530 mV subtractively normalized to 0 V. Left: Pt edge of air-breathing Pt cathode. Right: Ni edge of an air breathing PtNi cathode catalyst.

lerica, MA) and analyzed with Opus 6.5TM software. The potential dependent IR specular reflectance spectra of adsorbed CO (CO_{ads}) was obtained for CO dosing potentials (E_{ads}) of 100–400 mV vs. RHE in 100 mV increments. Prior to acquisition of the background IR spectrum, the cell was brought to 50 °C with H_2 (50 sccm) at the counter-reference electrode and N_2 at the working electrode (200 sccm) for 15 min. The working electrode feed was switched to CO (40 sccm) at the selected adsorption potential for 15 min prior to purging the working electrode with N_2 (200 sccm). The potential was set to 100 mV prior to acquisition of four signal-averaged (250 scans) spectra, at 50 mV increments, until the CO vibrational bands were no longer observable.

3. Results and discussion

3.1. Time dependent X-ray absorption spectroscopy

Fig. 5 shows time-dependent subtractively normalized XANES spectra of cathode catalytic layers of an air breathing hydrogen fuel cell operating at a temperature of 50 °C. Fig. 5 (left) shows the Pt time-dependent XANES (at 530 mV), each obtained as an average of three consecutive scans. The two peaks at 11553 eV and 11578 eV decrease with time, as the Pt is reduced, with a time-constant on the

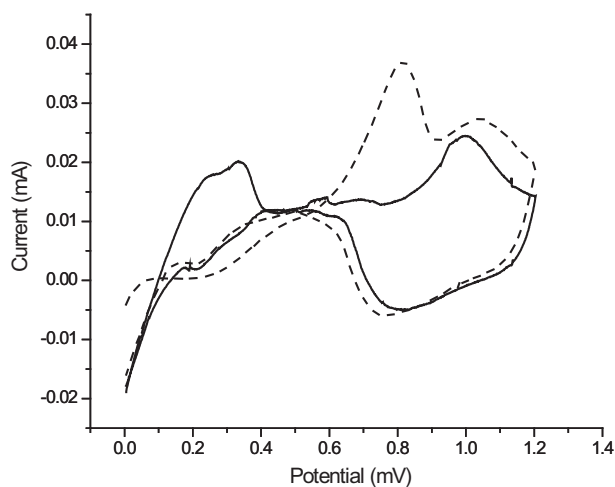


Fig. 6. Cyclic voltammetry (10 mV/s) of fuel cell working electrode (5-cm² geometric) under humidified nitrogen at 50 °C (solid). Humidified H_2 (50 sccm) at the counter-reference. CO stripping wave (dashed).

order of hours. The large time constant cannot be attributed solely to reduction of chemisorbed oxygen. The reduction of sub-surface oxygen, native to the crystallite core structure, may be responsible for the long time-constant. Stoupin et al. have shown that in the case of PtRu, the oxide phase extends into the core of particle [18]. A large Pt restructuring time-constant provides an explanation for the better performance obtained when acquiring cathode polarization curves from low to high potentials [46]. Fig. 5 (right) shows the Ni-edge time-dependent data, using the same experimental conditions as those on the left, from a PtNi/C cathode catalyst. This PtNi (1:1) was provided by ETEK. Jia et al. performed EXAFS fits of the same data [47], and attributed the shorter time constant for the Ni edge transient to the predominance of the Ni within the metal core:

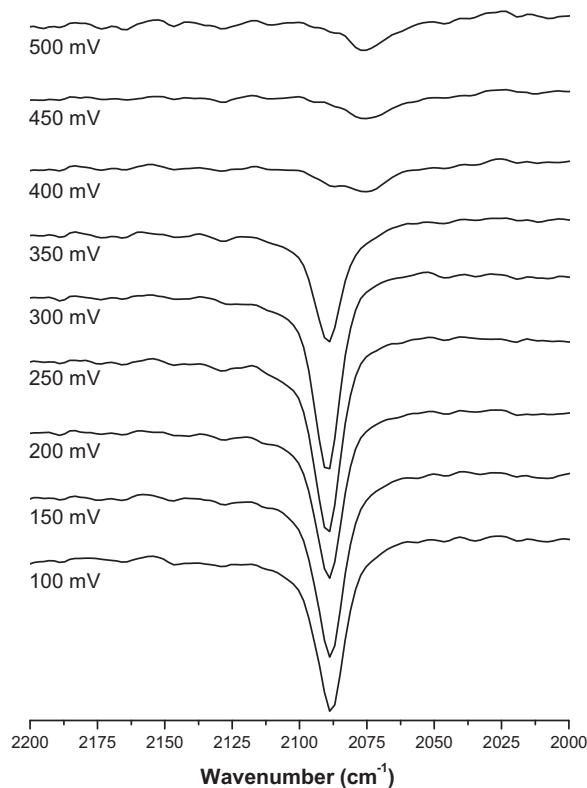


Fig. 7. Potential-dependent IR spectra of CO_{ads} on Pt with an adsorption potential of 100 mV.

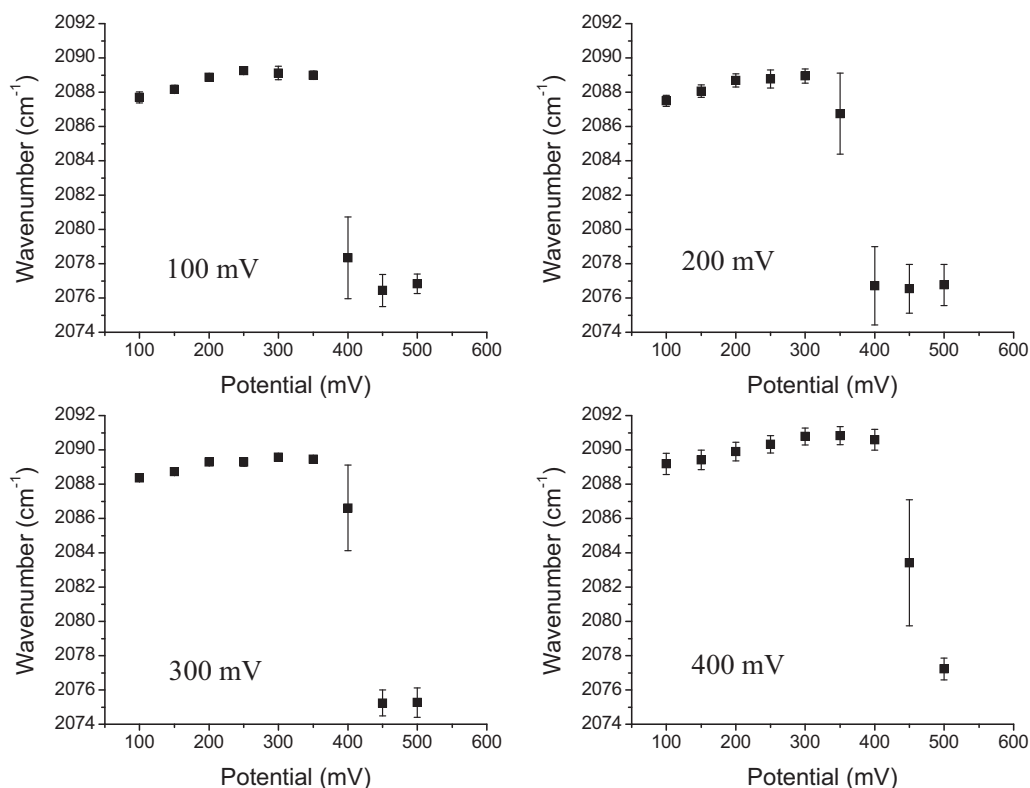


Fig. 8. Stark tuning plots of linearly adsorbed CO adsorbed on Pt.

the surface, dominated by Pt, has only small amounts of Ni available for adsorption/reduction of chemisorbed oxygen. The data of Fig. 5 suggests that a broad window of times constants is required for understanding time-dependent phenomena.

The time constants associated with the XAS of this work range from minutes to hours. Tada et al. [48], using transmission studies done on a Viswanathan-type cell reported a method for obtaining 1 s time-resolved full EXAFS spectra from a fuel cell being cycled between 0.4 and 1.0 V. They have observed separate time constants for charging and discharging, as well as the formation and dissociation of surface Pt–O bonds. Even shorter time constants will be possible using dispersive XAFS techniques and lifetime studies using catalysts kept in operation for hundreds of hours will become possible as operando fuel cells become more available.

3.2. Operando infrared spectroscopy of CO/Pt

Fig. 6 shows background CV (red) and the CO stripping wave (blue) obtained with the cell at 50 °C. The CO stripping wave, acquired at 10 mV/s, extends from about 600 to 900 mV. The potential dependent IR spectra of CO_{ads} at 100 mV vs. NHE are shown in Fig. 7. The peak positions vs. potential (Stark tuning plots) for CO adsorbed at 100, 200, 300 and 400 mV (Fig. 8) complement an operando temperature dependent study conducted by Kendrick et al. [49] and is similar to the data of Stamenkovic et al. studying CO on Pt(1 1 1) in 0.5 M H₂SO₄ [50]. The Stark tuning rates of this work, $6.8 \pm 0.6 \text{ cm}^{-1}/\text{mV}$, are within the range of $2.5 \text{ cm}^{-1}/\text{V}$ to $18.3 \text{ cm}^{-1}/\text{V}$ of previous operando Stark tuning studies of direct methanol fuel cells at potentials negative of 0.5 V vs. NHE [42]. The variations in fuel cell Stark tuning rates correlated with methanol concentration or CO coverage (e.g., when dosing the DMFC directly with CO). Stark tuning rates for MEA incorporated Pt are lower than those reported for polished polycrystalline Pt (e.g., $23.8 \text{ cm}^{-1}/\text{V}$ [51] to $27.5 \text{ cm}^{-1}/\text{V}$ [52]). The differences may be due to unique surface

conditions provided by the operando environment (e.g., MEA Pt is Nafion coated).

Stamenkovic correlated the complex Stark tuning of CO_{ads} stretching frequencies (ν_{CO}) to the compression/dissipation of CO_{ads} islands: A linear Stark tuning region with a subtle ν_{CO} blue shift from the extrapolated linear region was followed by a precipitous drop in ν_{CO} , followed by an upturn. The potential where ν_{CO} precipitously drops (E_{onset}) correlates with CO_{ads} oxidation. Stamenkovic identified the co-adsorbate as HSO₃[−] originating from the 0.5 M H₂SO₄ electrolyte used in their study. Kendrick, using no supplemental electrolyte (i.e., operando conditions), identified co-adsorbates as the Nafion sulfonate exchange group and the side chain CF₃ group. CO_{ads} oxidation, induced by OH[−] adsorp-

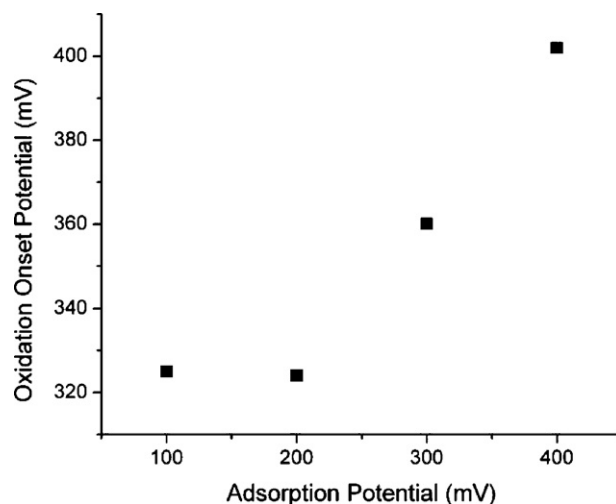


Fig. 9. CO electro-oxidation onset potentials vs. adsorption potentials.

tion, diminishes dipole–dipole coupling and thus precipitously decreases ν_{CO} . The upturn is ascribed to increased adsorption of sulfonate species relative to OH^- , which reestablishes repulsive dipole interactions that compress CO_{ads} islands and increases ν_{CO} .

Fig. 9 shows how E_{onset} depends on E_{ads} . At 400 mV, E_{onset} and E_{ads} coincide because at higher potentials CO_{ads} favors adsorption sites with higher enthalpies of adsorption (e.g., steps and kinks) [53,54] and there is no thermodynamic force driving migration to sites of lower ΔH_{ads} . At an E_{ads} of 300 mV, the E_{onset} exceeds E_{ads} by 60 mV because the distribution of adsorption sites are more heterogeneous and there is a driving force for CO_{ads} on terraces to migrate to steps, kinks and ad atoms. Thus the difference between E_{onset} on E_{ads} would be expected to increase as E_{ads} is decreased. At E_{ads} of 200 mV and lower, the E_{onset} is leveled to 320 mV.

4. Conclusion

An IR-XAS cell enables acquisition of X-ray absorption, and IR reflectance spectra of fuel cell catalysts and adsorbates with flowing fuel and oxidant gas streams at controlled cell temperatures (i.e., operando conditions). Time-dependent subtractively normalized XANES spectra show catalyst structural changes with time constants up to hours, explaining why better performance is observed with cathode polarization curves obtained from low to high potentials. Stark tuning of CO adsorbed at 100, 200, 300 and 400 mV vs. the fuel cell counter-reference electrode (i.e., NHE) is interpreted in terms of the difference between the oxidation onset potential and the potential at which the CO was adsorbed. At 400 mV, the oxidation onset potential (E_{onset}) is coincident with the adsorption potential (E_{ads}) because CO preferentially adsorbs only on sites with high ΔH_{ads} and there is no driving force for migration. As E_{ads} , E_{onset} decreases relative to E_{ads} as CO migrates to sites of higher enthalpies of adsorption. At E_{ads} at or below 200 mV the E_{onset} is leveled to 325 mV.

Acknowledgments

This work was funded by the Army Research Office DURIP grant and NuVant Systems Inc.

References

- [1] H. Topsøe, *Journal of Catalysis* 216 (2003) 155.
- [2] L. Ploense, M. Salazar, B. Gurau, E.S. Smotkin, *Journal of the American Chemical Society* 119 (1997) 11550.
- [3] L. Ploense, M. Salazar, B. Gurau, E.S. Smotkin, *Solid State Ionics* 136–137 (2000) 713.
- [4] M. Salazar, E.S. Smotkin, *Journal of Applied Electrochemistry* 36 (2006) 1237.
- [5] J.A. Mosko, *Analytical Chemistry* 56 (1984) 629.
- [6] S.T. Liu, Z.H. Chen, J.B. Xie, J.A. Lin, Z.J. Chen, P.F. Rao, *Analytical Chemistry* 82 (2010) 8544.
- [7] A. Motoyama, T. Xu, C.I. Ruse, J.A. Wohlschlegel, J.R. Yates, *Analytical Chemistry* 79 (2007) 3623.
- [8] S. Talwalkar, M. Chauhan, P. Aghalayam, Z.W. Qi, K. Sundmacher, S. Mahajani, *Industrial and Engineering Chemistry Research* 45 (2006) 1312.
- [9] Y. Roman-Leshkov, J.N. Chheda, J.A. Dumesic, *Science* 312 (2006) 1933.
- [10] Z.J. Liu, R.G. Arnold, E.A. Betterton, E. Smotkin, *Environmental Science and Technology* 35 (2001) 4320.
- [11] F. Rubel, *Design Manual: Removal of Arsenic from Drinking Water by Ion Exchange*, EPA/600/R-03/080, U.S. Environmental Protection Agency, Cincinnati, OH, 2003.
- [12] E.S. Smotkin, R.R. Diaz-Morales, *Annual Review of Materials Research* 33 (2003) 557.
- [13] S. Gottesfeld, T.A. Zawodzinski, R.C., in: Alkire H. Gerischer, D.M. Kolb, C.W. Tobias (Eds.), *Polymer Electrolyte Fuel Cells*, Wiley-VCH, 1997, vol. 5, p. 229.
- [14] L. Liu, C. Pu, B. Viswanathan, Q. Fan, R. Liu, E.S. Smotkin, *Electrochimica Acta* 43 (1998) 3657.
- [15] L. Liu, R. Viswanathan, R. Liu, E.S. Smotkin, *Electrochemical and Solid-State Letters* 1 (1998) 123.
- [16] P.T. Kissinger, W.R. Heineman, *Laboratory Techniques in Electroanalytical Chemistry*, 2nd ed., Marcel Dekker, Inc., New York, 1996, p. 199.
- [17] R. Viswanathan, R. Liu, E.S. Smotkin, *Review of Scientific Instruments* 73 (2002) 2124.
- [18] S. Stoupin, E.-H. Chung, S. Chattopadhyay, C.U. Segre, E.S. Smotkin, *Journal of Physical Chemistry B* 110 (2006) 9932.
- [19] E. Principi, A. Witkowska, S. Dsoke, R. Marassi, A. Di Cicco, *Physical Chemistry Chemical Physics* 11 (2009) 9987.
- [20] O. Petrova, C. Kulp, M.W.E. van den Berg, K.V. Klementiev, B. Otto, H. Otto, M. Lopez, M. Bron, W. Gruenert, *Review of Scientific Instruments* (2011) 82.
- [21] The first two digits are the equivalent weight of Nafion divided by 100; the last digit is the thickness of Nafion in thousandths of an inch.
- [22] H. Rivera, J.S. Lawton, D.E. Budil, E.S. Smotkin, *Journal of Physical Chemistry B* 112 (2008) 8542.
- [23] D. Wilkinson, Ballard Power Systems, Personal Communication, 1996.
- [24] B. Gurau, E. Smotkin, *Journal of Power Sources* 112 (2002) 339.
- [25] A. Bard, L. Faulkner, *Electrochemical Methods: Fundamentals and Applications*, John Wiley & Sons, 2001.
- [26] R. Buzzoni, S. Bordiga, G. Ricchiardi, G. Spoto, A. Zecchina, *Journal of Physical Chemistry* 99 (1995) 11937.
- [27] C. Roth, N. Benker, T. Buhrmester, M. Mazurek, M. Loster, H. Fuess, D.C. Koningsberger, D.E. Ramaker, *Journal of the American Chemical Society* 127 (2005) 14607.
- [28] R.J.K. Wiltshire, C.R. King, A. Rose, P.P. Wells, M.P. Hogarth, D. Thompsett, A.E. Russell, *Electrochimica Acta* 50 (2005) 5208.
- [29] C. Roth, N. Martz, T. Buhrmester, J. Scherer, H. Fuess, *Physical Chemistry Chemical Physics* 4 (2002) 3555.
- [30] F.J. Scott, C. Roth, D.E. Ramaker, *Journal of Physical Chemistry C* 111 (2007) 11403.
- [31] S. Maniguet, R.J. Mathew, A.E. Russell, *Journal of Physical Chemistry B* 104 (2000) 1998.
- [32] J. Singh, M. Tromp, O.V. Safonova, P. Glatzel, J.A. van Bokhoven, *Catalysis Today* 145 (2009) 300.
- [33] D.E. Ramaker, D.C. Koningsberger, *Physical Chemistry Chemical Physics* 12 (2010) 5514.
- [34] V. Croze, F. Ettingshausen, J. Melke, M. Soehn, D. Stuermer, C. Roth, *Journal of Applied Electrochemistry* 40 (2010) 877.
- [35] A.E. Russell, S. Maniguet, R.J. Mathew, J. Yao, M.A. Roberts, D. Thompsett, *Journal of Power Sources* 96 (2001) 226.
- [36] F.J. Scott, S. Mukerjee, D.E. Ramaker, *Journal of the Electrochemical Society* 154 (2007) A396.
- [37] M. Teliska, W.E. O'Grady, D.E. Ramaker, *Journal of Physical Chemistry B* 108 (2004) 2333.
- [38] M. Teliska, V.S. Murthi, S. Mukerjee, D.E. Ramaker, *Journal of Physical Chemistry C* 111 (2007) 9267.
- [39] M. Teliska, D.E. Ramaker, V. Srinivasamurthi, S. Mukerjee, *Proceedings: Electrochemical Society 2003–2030* (2005) 212.
- [40] C. Roth, D.E. Ramaker, in: C.G. Vayenas (Ed.), *Interfacial Phenomena in Electrocatalysis*, vol. 51, Springer, New York, 2011, p. 159.
- [41] Q. Fan, C. Pu, K.L. Ley, E.S. Smotkin, *Journal of the Electrochemical Society* 143 (1996) L21.
- [42] A.L. Bo, S. Sanicharane, B. Sompalli, Q.B. Fan, B. Gurau, R.X. Liu, E.S. Smotkin, *Journal of Physical Chemistry B* 104 (2000) 7377.
- [43] FTIR studies require a slot cut into the GDL to enable beam access to the catalytic surface.
- [44] M.S. Wilson, S. Gottesfeld, *Journal of Applied Electrochemistry* 22 (1992) 1.
- [45] S. Sanicharane, A. Bo, B. Sompalli, B. Gurau, E.S. Smotkin, *Journal of the Electrochemical Society* 149 (2002) A554.
- [46] V.S. Murthi, R.C. Urian, S. Mukerjee, *Journal of Physical Chemistry B* 108 (2004) 11011.
- [47] Q. Jia, E.A. Lewis, C. Grice, E.S. Smotkin, C.U. Segre, *Journal of Physics: Conference Series* 190 (2009) 12157.
- [48] M. Tada, S. Murata, T. Asasoka, K. Hiroshima, K. Okumura, H. Tanida, T. Uruga, H. Nakanishi, S. Matsumoto, Y. Inada, M. Nomura, Y. Iwasawa, *Angewandte Chemie International Edition* 46 (2007) 4310.
- [49] I. Kendrick, D. Kumari, A. Yakaboski, N. Dimakis, E.S. Smotkin, *Journal of the American Chemical Society* 132 (2010) 17611.
- [50] V. Stamenkovic, K.C. Chou, G.A. Somorjai, P.N. Ross, N.M. Markovic, *Journal of Physical Chemistry B* 109 (2005) 678.
- [51] R.X. Liu, H. Iddir, Q.B. Fan, G.Y. Hou, A.L. Bo, K.L. Ley, E.S. Smotkin, Y.E. Sung, H. Kim, S. Thomas, A. Wieckowski, *Journal of Physical Chemistry B* 104 (2000) 3518.
- [52] G.Q. Lu, A. Lagutchev, D.D. Dlott, A. Wieckowski, *Surface Science* 585 (2005) 3.
- [53] C.S. Kim, C. Korzeniewski, *Analytical Chemistry* 69 (1997) 2349.
- [54] J. Yoshinobu, N. Tsukahara, F. Yasui, K. Mukai, Y. Yamashita, *Physical Review Letters* 90 (2003) 248301.